Methyl Transfer in Glucosinolate Biosynthesis Mediated by Indole Glucosinolate *O*-Methyltransferase 5[1]

Marina Pfalz, Maisara Mukhaimar, François Perreau, Jayne Kirk, Cecilie Ida Cetti Hansen, Carl Erik Olsen, Niels Agerbirk, and Juergen Kroymann*

Ecologie Systématique Evolution, Centre National de la Recherche Scientifique/Université Paris-Sud/AgroParisTech, Université Paris-Saclay, 91400 Orsay, France (M.P., M.M., J.Kr.); Palestinian National Agricultural Research Center, 19356 Jenin, Palestine (M.M.); Institut Jean-Pierre Bourgin, Institut National de la Recherche Agronomique/AgroParisTech/Centre National de la Recherche Scientifique, Université Paris-Saclay, 78000 Versailles, France (F.P.); Waters, Ltd., Wilmslow SK9 4AX, United Kingdom; and Copenhagen Plant Science Center and Department of Plant and Environmental Sciences, University of Copenhagen, 1165 Copenhagen, Denmark (C.I.C.H., C.E.O., N.A.)

ORCID IDs: 0000-0003-2388-9714 (M.M.); 0000-0001-7873-9866 (F.P.); 0000-0002-2275-0596 (C.E.O.); 0000-0003-4670-8330 (N.A.); 0000-0002-4573-6498 (J.Kr.).

Indole glucosinolates (IGs) are plant secondary metabolites that are derived from the amino acid tryptophan. The product of Arabidopsis (*Arabidopsis thaliana*) IG core biosynthesis, indol-3-ylmethyl glucosinolate (I3M), can be modified by hydroxylation and subsequent methoxylation of the indole ring in position 1 (1-IG modification) or 4 (4-IG modification). Products of the 4-IG modification pathway mediate plant-enemy interactions and are particularly important for Arabidopsis innate immunity. While *CYP81F*s encoding cytochrome P450 monooxygenases and *IGMT*s encoding indole glucosinolate *O*-methyltransferases have been identified as key genes for IG modification, our knowledge about the IG modification pathways is not complete. In particular, it is unknown which enzyme is responsible for methyl transfer in the 1-IG modification pathway and whether this pathway plays a role in defense, similar to 4-IG modification. Here, we analyze two Arabidopsis transfer DNA insertion lines with targeted metabolomics. We show that biosynthesis of 1-methoxyindol-3-ylmethyl glucosinolate (1MOI3M) from I3M involves the predicted unstable intermediate 1-hydroxyindol-3-ylmethyl glucosinolate (1OHI3M) and that *IGMT5*, a gene with moderate similarity to previously characterized *IGMT*s, encodes the methyltransferase that is responsible for the conversion of 1OHI3M to 1MOI3M. Disruption of IGMT5 function increases resistance against the root-knot nematode *Meloidogyne javanica* and suggests a potential role for the 1-IG modification pathway in Arabidopsis belowground defense.

Glucosinolates are nitrogen- and sulfur-containing secondary metabolites found in Arabidopsis (*Arabidopsis thaliana*) and related plants. About 132 different glucosinolate structures were scientifically documented by 2011 (Agerbirk and Olsen, 2012). Glucosinolate biosynthesis from amino acids involves conversion of the amino acid to an oxime, addition of a thiol group and subsequent formation of a β-thioglycosidic bond with Glc, and finally sulfation of the oxime group (Sønderby et al., 2010). This reaction sequence results in the formation of the glucosinolate core structure, which then can undergo further modification reactions (for review, see Halkier and Gershenzon, 2006). In Arabidopsis, three classes of these β-D-thioglucoside-*N*-hydroxysulfates are present: Met-derived aliphatic, Phe-derived benzenic, and Trp-derived indole glucosinolates (IGs).

IGs have multiple functions in defense against a wide range of enemies, including leaf-clipping and phloem-feeding arthropods (Kim and Jander, 2007; de Vos et al., 2008; Kim et al., 2008; Pfalz et al., 2009; Sun et al., 2009), nonhost fungal and nonhost bacterial pathogens (Bednarek et al., 2009; Clay et al., 2009), and fungal pathogens via conversion to phytoalexins (Pedras et al., 2010, 2011). From a nutritional perspective, IGs also are of interest, but very little is known of the effect of those substitutions of the indole moiety that are commonly found in vegetables such as broccoli (*Brassica oleracea*) and several other cabbages (*Brassica* spp.; Agerbirk et al., 2009; Latté et al., 2011).

Four IGs differing in the substitutions of the indole moiety are commonly present in Arabidopsis

[1] This work was supported by the Agence National de la Recherche (grant no. ANR-10-GENM-005 to J.Kr.), the European Commission (grant no. FP7-People-2009-IEF 253272 to M.P.), the Consulate General of France in Jerusalem (fellowship to M.M.), and LabEx Saclay Plant Sciences (grant no. ANR-10-LABX-0040-SPS to the Institut Jean-Pierre Bourgin).

* Address correspondence to juergen.kroymann@u-psud.fr.

The author responsible for distribution of materials integral to the findings presented in this article in accordance with the policy described in the Instructions for Authors (www.plantphysiol.org) is: Juergen Kroymann (juergen.kroymann@u-psud.fr).

J.Kr. and M.P. conceived this project; M.P., M.M., F.P., J.Ki., C.I.C.H., C.E.O., and N.A. performed experiments; J.Kr., M.P., F.P., J.Ki., C.I.C.H., C.E.O., and N.A. analyzed data; J.Kr. wrote the article with contributions from N.A., M.P., M.M., and F.P.

www.plantphysiol.org/cgi/doi/10.1104/pp.16.01402

 © 2016 American Society of Plant Biologists. All Rights Reserved.

and cabbages. Those are indol-3-ylmethyl (I3M), 1-methoxyindol-3-ylmethyl (1MOI3M), 4-hydroxyindol-3-ylmethyl (4OHI3M), and 4-methoxyindol-3-ylmethyl (4MOI3M) glucosinolates. Biosynthesis of the glucosinolate core structure from Trp results in the formation of I3M, which subsequently can be modified at position 1 or 4 of the indole ring. I3M is the prevailing IG in Arabidopsis leaves and seeds, while 1MOI3M dominates root IG profiles (Kliebenstein et al., 2001a; Petersen et al., 2002; Brown et al., 2003; Pfalz et al., 2011). Data supporting the existence of an additional, supposedly unstable, Arabidopsis IG, 1-hydroxyindol-3-ylmethyl glucosinolate (1OHI3M), was presented recently (Pfalz et al., 2011), but direct evidence for the presence of this metabolite in Arabidopsis is still required.

Key enzymes for the modification of I3M are cytochrome P450 monooxygenases of the CYP81F subfamily and indole glucosinolate *O*-methyltransferases (IGMTs) of plant *O*-methyltransferase family 2. CYP81Fs introduce hydroxy groups at specific positions of the indole ring of I3M, and IGMTs convert hydroxy to methoxy groups (Pfalz et al., 2009, 2011). The Arabidopsis genome contains four *CYP81F* genes. *CYP81F1*, *CYP81F3*, and *CYP81F4* form a cluster on chromosome 4, while *CYP81F2* is located on chromosome 5. In a transient *Nicotiana benthamiana* expression system, CYP81F1 to CYP81F3 were capable of catalyzing hydroxylation at position 1 and 4 of the indole ring, whereas CYP81F4 hydroxylated only the nitrogen (N) at position 1. Noteworthy, the 1-hydroxylated product, 1OHI3M, was not detected directly in these experiments but could be deduced from the presence of 1MOI3M when *CYP81F*s were coexpressed with *IGMT*s. Analyses of Arabidopsis *cyp81f* mutants, however, revealed a more restricted enzymatic specificity of CYP81F1 to CYP81F3 and supported only their participation in the position 4 (4-IG) modification pathway (Pfalz et al., 2011).

Four tandemly arranged *IGMT* genes (*IGMT1–IGMT4*) cluster on the left arm of chromosome 1. Their gene products share more than 94% identity. IGMT1 and IGMT2 were shown to be capable of converting 4OHI3M and 1OHI3M to 4MOI3M and 1MOI3M, respectively, when coexpressed with the IG core pathway genes and with *CYP81F*s in *N. benthamiana* (Pfalz et al., 2011). However, the Arabidopsis genome contains an additional putative *IGMT*. This gene, tentatively named *IGMT5*, is located separate from the other four *IGMT*s on the right arm of chromosome 1, and its gene product shares only about 70% identity with IGMT1 to IGMT4. Accordingly, IGMT1 to IGMT4 and IGMT5 branched as sister clades in a genealogy of Arabidopsis *O*-methyltransferases (Kim et al., 2005). Because *IGMT5* expression correlated strongly with *CYP81F4* expression across tissues and treatments (Pfalz et al., 2011), we speculated that this *O*-methyltransferase may play a role in 1-IG modification.

Here, we show that *IGMT5* indeed participates in the 1-IG modification pathway, based on targeted metabolomics of two Arabidopsis lines with a T-DNA inserted into the *IGMT5* promoter. We demonstrate that the proposed, but to date rather elusive, substrate of IGMT5, 1OHI3M, exists. We show that disruption of the IGMT5 function in roots leads to a strong reduction of 1MOI3M abundance, a concomitant accumulation of 1OHI3M, and the formation of previously undetected IG derivatives. Finally, we uncover an unexpected role of *IGMT5* in defense against the plant-parasitic root-knot nematode *Meloidogyne javanica*.

RESULTS

T-DNA Insertions in the *IGMT5* Promoter Alter *IGMT5* Expression

To test the hypothesis that IGMT5 participates in IG modification, we investigated two independent Arabidopsis T-DNA insertion lines, SALK_151470 (Alonso et al., 2003) and GK_390B09 (Kleinboelting et al., 2012). Both lines are in the Columbia-0 (Col-0) background and have a T-DNA inserted into the promoter region of *IGMT5*, approximately 800 bp upstream of the *IGMT5* start codon in SALK_151470 and approximately 160 bp upstream of the start codon in GK_390B09 (Fig. 1). Mutant plants displayed no visible phenotypic alterations from the Col-0 wild type, and mutant growth rate did not differ from that of the wild type. To test whether the T-DNA insertions influenced *IGMT5* expression, we analyzed leaf and root transcripts of mutant and wild-type plants with real-time quantitative PCR (RT-qPCR) in two independent experiments, each with at least three biological replicates per genotype and tissue. Wild-type roots accumulated significantly more *IGMT5* transcript than leaves (Figs. 2 and 3). Leaf *IGMT5* transcript levels in both mutants were significantly higher than in the wild type, by more than 2 orders of magnitude in SALK_151470 (Fig. 2A) and by about 1 order of magnitude in GK_390B09 (Fig. 3A). Hence, both T-DNA insertion lines overexpressed *IGMT5* in their leaves ($IGMT5_{L\text{-}OE}$). By contrast, the effect of the T-DNAs on root *IGMT5* transcript levels differed between insertion lines. While SALK_151470 roots accumulated about 5-fold more *IGMT5* transcript than the wild type (Fig. 2A), *IGMT5* expression in GK_390B09 roots was strongly reduced, to about 2% of the wild-type level (Fig. 3A). Thus, SALK_151470 overexpressed *IGMT5* in roots ($IGMT5_{R\text{-}OE}$) while GK_390B09 had *IGMT5* knocked out in this organ ($igmt5_{R\text{-}KO}$). Leaf or root transcript levels of the other *IGMT* genes, *IGMT1* to *IGMT4*, were not substantially affected by the T-DNA insertions in the *IGMT5* promoter. There was also no effect on *CYP81F4* expression; transcript analysis by RT-qPCR confirmed the previously reported expression pattern (Pfalz et al., 2011), with low *CYP81F4* transcript abundance in leaves and high abundance in roots (Figs. 2A and 3A).

T-DNA Insertions in the *IGMT5* Promoter Alter IG Composition

The composition of aliphatic glucosinolates in both T-DNA insertion mutants was typical for a Col-0

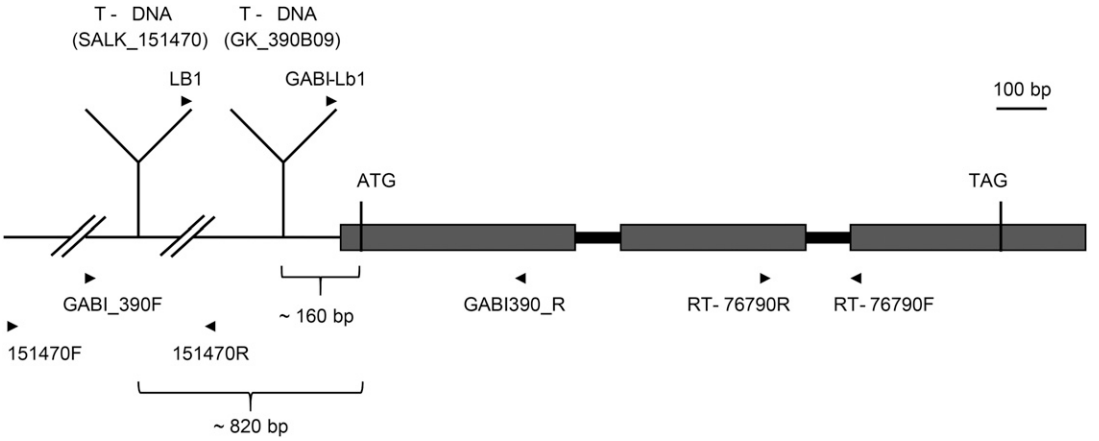

Figure 1. The *IGMT5* gene in Arabidopsis. Shown are exons (gray bars), introns (black bars), and the promoter region (black line). Start and stop codons are indicated by vertical black lines. The promoter region is not drawn to scale. The locations of T-DNA insertions in SALK_151470 and GK_390B09 are indicated by Y-shaped lines. Primer positions are indicated by small black triangles.

genetic background, determined largely by a *MAM1* allele at the *GS-Elong* locus and an *AOP1* allele at the *GS-AOP* locus (Magrath et al., 1994; Giamoustaris and Mithen, 1996; Kliebenstein et al., 2001a, 2001b; Kroymann et al., 2001, 2003). Compared with the Col-0 wild type, methylsulfinylalkyl glucosinolates seemed slightly elevated in GK_390B09 roots, but these effects were not statistically significant, except for 6-methylsulfinylhexyl glucosinolate ($F_{1,30}$ = 10.51, $P < 0.01$), an aliphatic glucosinolate present in minor amounts. By contrast, IG profiles displayed substantial alterations compared with the wild type (Figs. 2B and 3B). In SALK_151470 (with the $IGMT5_{R\text{-}OE}$ genotype), there was a 50% increase in 1MOI3M concentration ($F_{1,19}$ = 5.24, $P < 0.05$), while the levels of other IGs were unaltered. In GK_390B09 ($igmt5_{R\text{-}KO}$), 1MOI3M root concentration was reduced to less than 2% of the wild-type level ($F_{1,30}$ = 390.7, $P < 10^{-8}$), whereas I3M and 4MOI3M concentrations were elevated significantly (both $F_{1,30} > 19$, $P < 10^{-3}$). Furthermore, *igmt5* roots accumulated three additional compounds, termed c1, c2, and c3, which had not been detected previously in glucosinolate extracts. Compounds c1 and c2 had UV light absorption spectra typical for IGs, with a peak around 220 nm and a broad shoulder from 260 to 300 nm (Supplemental Fig. S1). These features also were present in the UV light profile of c3 but were accompanied by a dominant peak at 200 nm, suggesting that an additional, aromatic moiety was present in the c3 molecule. Furthermore, c1 was unstable; its concentration decreased over the time of HPLC analysis (Supplemental Fig. S2), suggesting that intact mutant roots accumulated more of this compound than we were able to detect.

Surprisingly, leaves of GK_390B09 ($IGMT5_{L\text{-}OE}$) accumulated only approximately 50% of wild-type 1MOI3M ($F_{1,31}$ = 70.2, $P < 10^{-8}$; Fig. 3B), whereas the 1MOI3M concentration increased in leaves of SALK_151470 (also $IGMT5_{L\text{-}OE}$). This increase was moderate, approximately 25%, but nonetheless statistically significant ($F_{1,37}$ = 4.71, $P < 0.05$; Fig. 2B). None of the three newly discovered compounds was detectable in SALK_151470 (Fig. 2B), but c3 was present in the leaves of GK_390B09 (Fig. 3B). Leaf quantities of I3M, 4OHI3M, and 4MOI3M did not differ statistically between the mutants and the wild type. Likewise, aliphatic glucosinolate profiles did not differ between mutant and wild-type leaves.

The Newly Discovered Metabolites in *igmt5* Roots Are *N*-Hydroxy I3M and Two Derivatives

The postulated pathway for 1-IG modification, with *CYP81F4* converting I3M to 1OHI3M and an IGMT converting 1OHI3M to 1MOI3M (Pfalz et al., 2011), predicts that a block of the responsible IGMT function should result in accumulation of the methyltransferase substrate 1OHI3M and depletion of the reaction product 1MOI3M. We used mass spectrometry (MS), including ion-trap HPLC-MS and high-resolution mass spectrometry (HR-MS), to test these predictions and also to characterize the newly discovered metabolites.

Ion-trap HPLC-MS and tandem mass spectrometry (MS/MS) of desulfated glucosinolates confirmed that the strongly reduced IG in mutant roots was 1MOI3M (Supplemental Fig. S3). Furthermore, HR-MS of intact glucosinolates showed that one of the three newly discovered root compounds, c1, had the *m/z* of 463.0471 expected for $[1OHI3M - H]^-$, within the usual experimental error (Fig. 4; Table I). Importantly, 4OHI3M, whose anion has the same *m/z* value, eluted significantly earlier than c1 (Supplemental Figs. S1 and S3). Analysis of desulfated glucosinolates by HPLC with high-resolution quadrupole-time of flight MS and with ion-trap MS/MS detection (Supplemental Fig. S3) confirmed this result and provided further evidence: while the desulfo derivative of 4OHI3M did not lose a

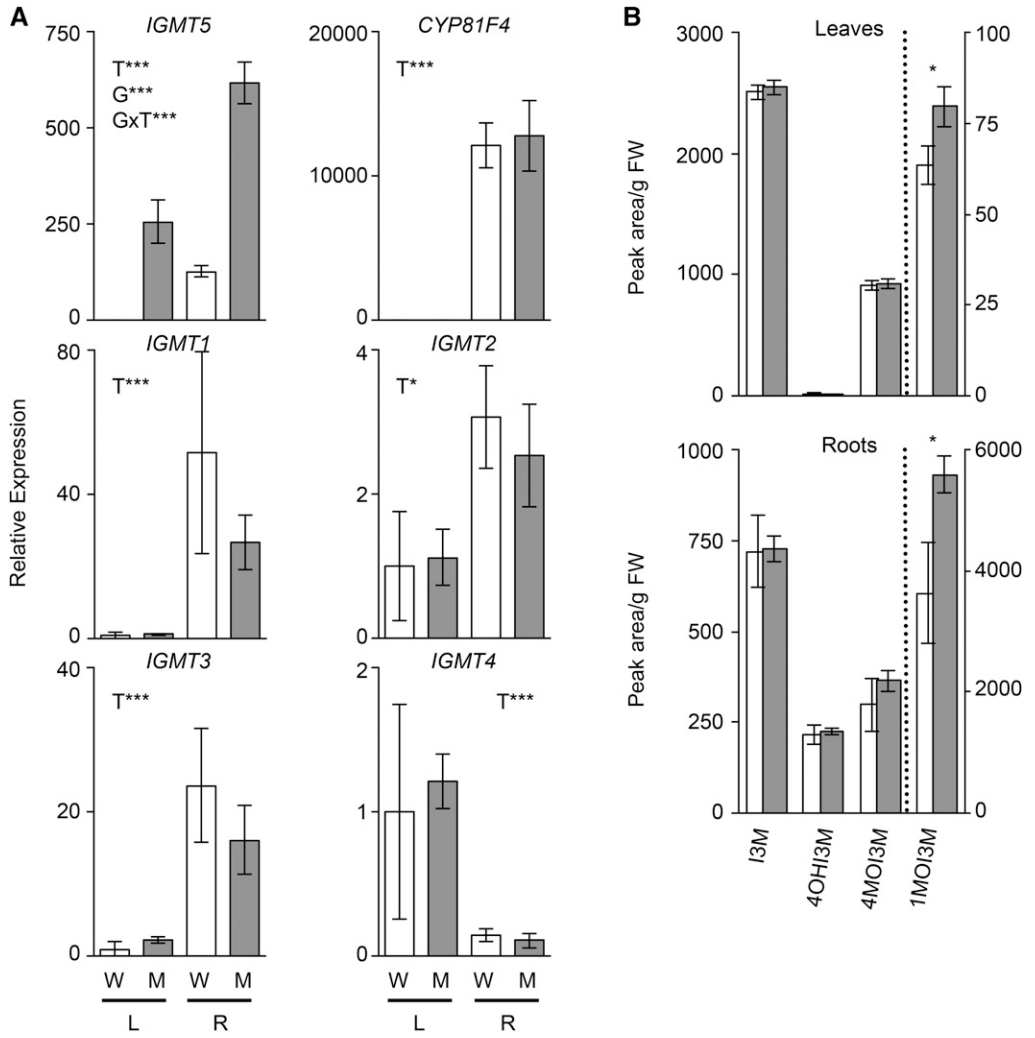

Figure 2. Altered expression of *IGMT5* in SALK_151470 increases 1MOI3M concentration in leaves and roots. A, RT-qPCR analysis of *IGMT* and *CYP81F4* transcripts using RNA from leaves (L) and roots (R) of wild-type (W; white bars) and SALK_151470 (M; gray bars) plants. Transcript levels were normalized relative to the mRNA levels of *UBIQUITIN10*. For each genotype and tissue, at least three biological replicates were used ($3 \leq n \leq 8$). Expression values for wild-type leaves were set as 1; error bars show SE. Data were analyzed with ANOVA: expression = constant + genotype + tissue + genotype × tissue. Statistical significance for differences in transcript levels is indicated for genotype (G), tissue (T), and the interaction between genotype and tissue (G×T): *, $P < 0.05$; and ***, $P < 0.001$. B, IG profiles in the Arabidopsis wild type and SALK_151470. IG profiles were assessed in leaves and roots of Arabidopsis wild-type (white bars) and SALK_151470 mutant (gray bars) plants. *, $P < 0.05$. Per genotype and tissue, at least seven biological replicates were used ($7 \leq n \leq 32$); error bars show SE. Note that we used a different scale for 1MOI3M. FW, Fresh weight.

hydroxyl (OH) radical in ion-trap MS/MS, this was the major loss observed for desulfated c1, consistent with the hydroxyl group being attached to the indole N and, therefore, more susceptible to fragmentation. Therefore, we conclude that c1 corresponded to 1OHI3M.

HR-MS^2 spectra of compounds c2 and c3 displayed several ions diagnostic for glucosinolates (Fig. 4; Table I; Supplemental Fig. S3), confirming that c2 and c3 were glucosinolate derivatives. Compound c2 had an *m/z* of 625, but ions of *m/z* 463 and *m/z* 447 also were present in simple MS. These ions with *m/z* 463 and *m/z* 447 matched the expected masses of $[1OHI3M - H]^-$ and $[I3M - H]^-$. The *m/z* differences of 162 and 178 corresponded to anhydro-Glc and Glc (or an isomeric hexose), indicating that fragmentation of c2 occurred on both sides of an oxygen involved in a glycoside bond to Glc or another hexose. These data suggested that compound c2 is a glycosylated derivative of 1OHI3M, with the additional hexoside attached to the indole N via an oxygen atom and thus substituting the unstable *N*-hydroxy group. In the following, we refer to this compound as *N*-Hex-I3M.

Finally, c3 had a mass of *m/z* 659, and HR-MS suggested a molecular formula of $C_{26}H_{31}N_2O_{14}S_2$. HR-MS^2 spectra of this compound contained the fragment of *m/z* 447 typical for IGs, in addition to other ions diagnostic

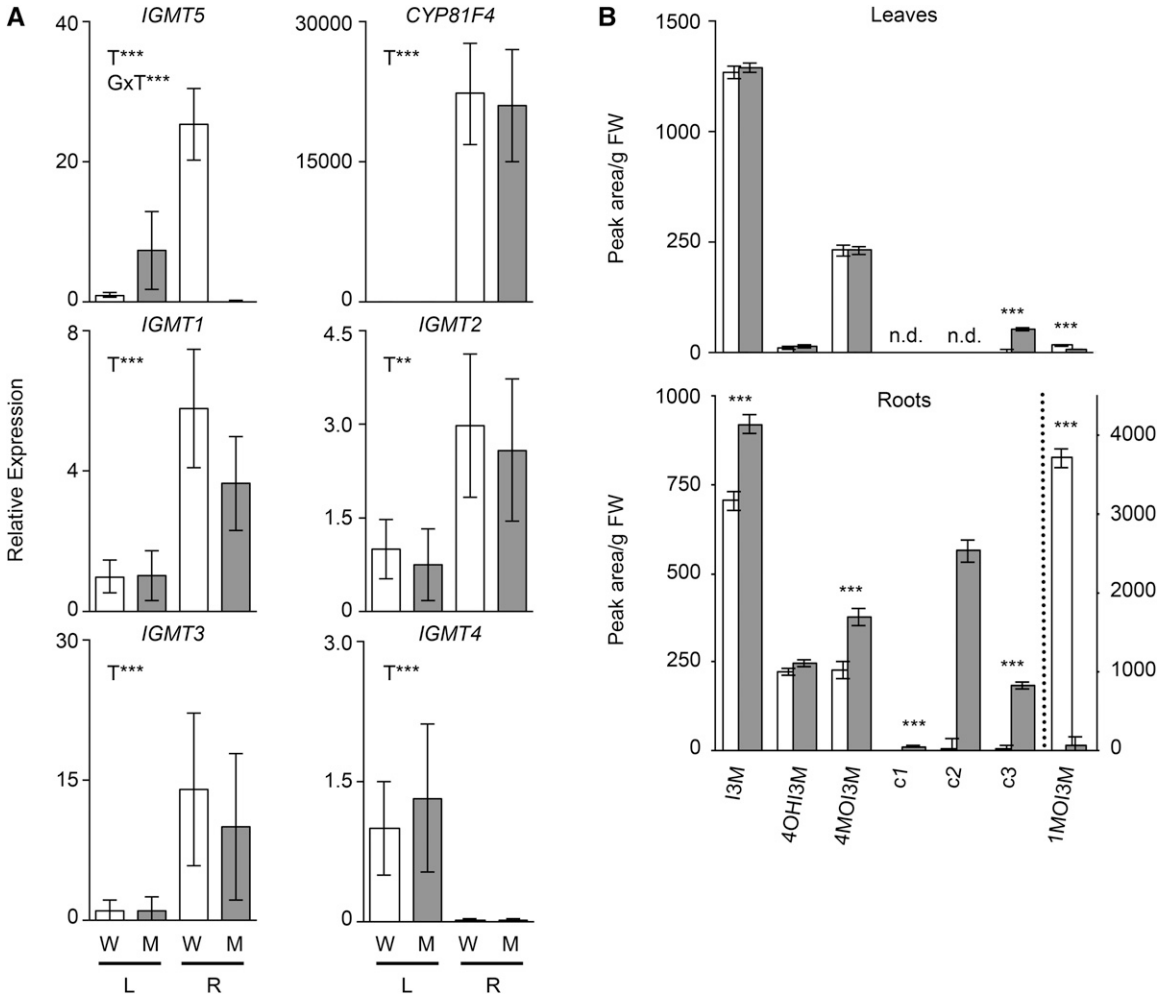

Figure 3. Altered expression of *IGMT5* in GK_390B09 has tissue-specific effects on leaf and root IG profiles. A, RT-qPCR analysis of *IGMT* and *CYP81F4* transcripts using RNA from leaves (L) and roots (R) of wild-type (W; white bars) and GK_390B09 (M; gray bars) plants. Transcript levels were normalized relative to the mRNA levels of *UBIQUITIN10*. For each genotype and tissue, three biological replicates were used ($n = 3$). Expression values for wild-type leaves were set as 1; error bars show SE. Data were analyzed with ANOVA: expression = constant + genotype + tissue + genotype × tissue. Statistical significance for differences in transcript levels is indicated for genotype (G), tissue (T), and the interaction between genotype and tissue (G×T): **, $P < 0.01$; and ***, $P < 0.001$. B, IG profiles in the Arabidopsis wild type and GK_390B09. IG profiles were assessed in leaves and roots of Arabidopsis wild-type (white bars) and GK_390B09 mutant (gray bars) plants. ***, $P < 0.001$; and n.d., not detected. Per genotype and tissue, 23 or 24 biological replicates were used; error bars show SE. Note that we used a different scale for 1MOI3M root concentration. Note also that the bars underestimate the true quantity of the unstable compound c1. FW, Fresh weight.

for glucosinolates. HR-MS of the corresponding desulfoglucosinolate agreed with the deduced molecular formula (found, 581.1795; calculated for $C_{26}H_{32}N_2O_{11}S$, 581.1800; Supplemental Fig. S3). From the biochemical context, molecular formula, and UV light spectrum, our working hypothesis for c3 was a structure based on I3M but with an O-$C_{10}H_{13}O_4$ radical at the indole N. Fragmentation of desulfo-c3 in MS^2 supported the presence of this substituent at the indole N. Losses corresponding to Glc and anhydro-Glc were observed (Supplemental Fig. S3), meaning that the substituent could not be attached at the thio-Glc moiety (Agerbirk and Olsen, 2011). A loss corresponding to 212 (substituent radical – hydrogen) was observed from the sodium adduct, meaning that the additional mass compared with that of I3M was in the form of a single substituent. Indeed, a known N derivative of I3M, 1MOI3M, likewise fragmented at the indole N in the ion trap, as opposed to 4MOI3M (Supplemental Fig. S3). While 1MOI3M lost an odd electron CH_3O radical, c3 lost the radical minus hydrogen (loss of $OC_{10}H_{12}O_4$, with mass 212). This MS^2 result is compatible with an N-O-C connected radical with the ability to form an aldehyde, allowing hydrogen transfer to the indole N. The deduced radical with a mass of 213 and predicted formula O-$C_{10}H_{13}O_4$ from both MS^2 and HR-MS of the intact and desulfated glucosinolate c3 would fit a trihydroxy-methoxy-phenylpropane-*O* moiety as well as a number of other

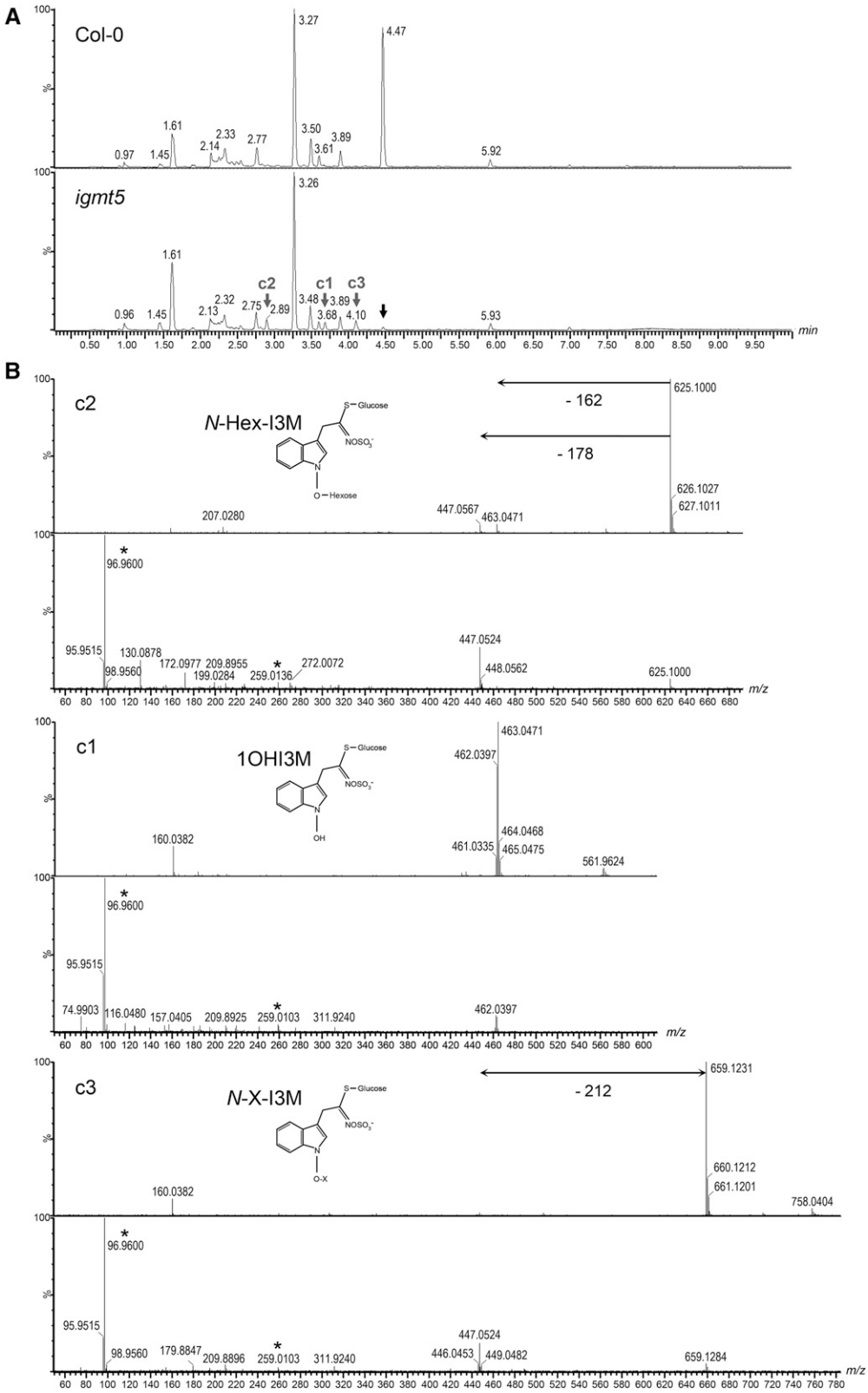

Figure 4. HR-MS of root extracts from the wild type and GK_390B09 (*igmt5*$_{R\text{-}KO}$). A, Ultra-performance liquid chromatography separation of root extracts from the wild type (Col-0) and mutant. Shown are HSO_4^- ion currents, which are characteristic for glucosinolates. Numbers next to peaks indicate retention times in minutes. Vertical arrows indicate peaks that differ between the wild type and mutant; gray, present in the mutant (c2, c1, and c3); black, strongly reduced in the mutant (1MOI3M). B, HR-MS and MS^2 spectra of c2, c1, and c3, and proposed chemical structures. Numbers

Table I. *HR-MS of newly discovered compounds c1, c2, and c3*

Method	Compound			Experimental *m/z*	Elemental Composition	Theoretical *m/z*	Error	Error	Interpretation/Remark
	c1	c2	c3						
							ppm	*D*	
MS			x	659.1231	$[C_{26}H_{31}N_2O_{14}S_2]^-$	659.1217	2.2	0.0014	$[(OHI3M + C_{10}H_{12}O_4) - H]^-$
		x		625.1000	$[C_{22}H_{29}N_2O_{15}S_2]^-$	625.1009	1.4	0.0009	$[(I3M + Glc) - H]^-$
	x	x		463.0471	$[C_{16}H_{19}N_2O_{10}S_2]^-$	463.0481	2.2	0.0010	$[OHI3M - H]^-$
		x		447.0567	$[C_{16}H_{19}N_2O_9S_2]^-$	447.0532	7.8	0.0035	$[I3M - H]^-$
		x		207.0280					
	x		x	160.0382	$[C_9H_6O_2N]^-$	160.0399	10.6	0.0017	
MS^2		x	x	447.0524	$[C_{16}H_{19}N_2O_9S_2]^-$	447.0532	1.8	0.0008	$[I3M - H]^-$
	x		x	311.9240					
	x			274.9908	$[C_6H_{11}O_8S_2]^-$	274.9895	4.7	0.0013	Diagnostic for glucosinolates[a]
		x		270.0072					
	x	x	x	259.0136	$[C_6H_{11}O_9S]^-$	259.0124	4.6	0.0012	Diagnostic for glucosinolates[a]
	x			240.9996	$[C_6H_9O_8S]^-$	241.0018	9.1	0.0022	Diagnostic for glucosinolates[a]
	x	x	x	209.8955					
		x		199.0284					
			x	179.8847					
		x		172.0977	$[C_8H_{14}NO_3]^-$	172.0974	1.7	0.0003	
	x			157.0405					
		x		130.0878	$[C_6H_{12}NO_2]^-$	130.0868	7.7	0.0010	
	x			116.0480					
	x	x	x	96.9600	HSO_4^-	96.9596	4.1	0.0004	Diagnostic for glucosinolates[a]
	x		x	74.9903	$[HOC_2H_2S]^-$	74.9904	1.3	0.0003	Diagnostic for glucosinolates[b]

[a]From Fabre et al. (2007). [b]From Bialecki et al. (2010).

isomers. In conclusion, MS^2 of desulfo-c3 supported the deduced molecular formula from HR-MS of intact c3, $[M - H]^- = C_{26}H_{31}O_{14}N_2S_2$, and a structure as I3M substituted with an O-$C_{10}H_{13}O_4$ radical at the indole N. We refer to this compound as *N*-X-I3M.

The desulfated derivatives of *N*-Hex-I3M (=c2) and *N*-X-I3M (=c3) were isolated successfully by preparative HPLC, but in three independent attempts, both were lost during lyophilization for solvent change before NMR. Residual NMR signals did not allow any conclusions regarding the compound identities. As a known desulfoglucosinolate (desulfo 4-methylsulfinylbutyl glucosinolate) used as positive control was stable during the procedure, and as a number of desulfated IG derivatives had been isolated previously at essentially identical conditions (Agerbirk et al., 2001; Agerbirk and Olsen, 2011), losses were attributed to a particular instability of desulfo *N*-Hex-I3M and desulfo *N*-X-I3M. Attempted isolation as intact glucosinolates *N*-Hex-I3M and *N*-X-I3M, in order to avoid the apparently destabilizing sulfatase treatment, also was unsuccessful despite using a gentle, well-established procedure (Agerbirk et al., 2014).

Mutations in *IGMT5* But Not *CYP81F4* Affect Resistance against *M. javanica*

We challenged Arabidopsis with the root-knot nematode *M. javanica* to test whether the 1-IG modification pathway had a potential impact on plant-parasite interactions. *M. javanica* is a soil-borne generalist plant parasite capable of completing its life cycle on Arabidopsis (Wu et al., 1998). Successful invasion of root tissue by juvenile root-knot nematodes induces the formation of root galls, in which the nematodes mature and reproduce.

We inoculated $igmt5_{R\text{-}KO}$ (GK_390B09), *cyp81f4* (SALK_024438), *cyp81f2* (SALK_005882), and Col-0, the common genetic background of the three mutants, with juvenile nematodes ($n = 10$ replicates per genotype). The *cyp81f4* mutant was defective in the conversion of I3M to 1OHI3M in the 1-IG modification pathway, indicated by the nearly complete absence of 1MOI3M (Pfalz et al., 2011). Similar to the $igmt5_{R\text{-}KO}$ genotype, *cyp81f4* roots had higher levels of 4OHI3M, 4MOI3M, and I3M than the wild type (Pfalz et al., 2011). The *cyp81f2* mutant was impaired in the conversion of I3M to 4OHI3M in the 4-IG modification pathway (Pfalz et al., 2009). Roots of this mutant displayed an approximately 50% reduction in the concentration of 4OHI3M and 4MOI3M and a moderate increase of I3M, but 1MOI3M content was indistinguishable from that of the wild type (Pfalz et al., 2011).

One month after inoculation, we counted the total number of nematode-induced root galls. On the Col-0 wild type, we found that, on average, approximately

Figure 4. (*Continued.*)
indicate observed *m/z* values. Stars indicate diagnostic ions for glucosinolates present in all three MS^2 spectra. Horizontal arrows indicate major shifts in *m/z* caused by substituent loss.

0.9 galls had developed per nematode in the inoculum, indicating a high rate of infection and nematode establishment. Root gall numbers differed significantly among genotypes ($F_{3,36} = 8.62$, $P < 0.0002$). The $igmt5_{R\text{-}KO}$ mutant had the lowest number of root galls, whereas *cyp81f2* and *cyp81f4* were indistinguishable from the wild type (Fig. 5). We confirmed these results (except for *cyp81f2*, which had germination problems) in an independent experiment (n = 10–30 replicates per genotype). We analyzed the combined results from both experiments with a mixed-model ANOVA, treating genotype as a fixed effect and experiment and genotype × experiment interaction as random effects to obtain mean squares (*MS*) for genotype and genotype × experiment in the model: gall number = constant + genotype + experiment + genotype × experiment. We calculated F ratios as $MS_{genotype}/MS_{genotype \times experiment}$. The genotype effect was significant ($F_{2,2} = 25.02$, $P < 0.05$), and $igmt5_{R\text{-}KO}$ had, on average, approximately 20% fewer galls than the wild type or *cyp81f4*, while gall numbers were indistinguishable between the wild type and *cyp81f4*. Hence, disruption of IGMT5 function ($igmt5_{R\text{-}KO}$), but not the absence of the entire 1-IG modification pathway (*cyp81f4*), attenuated nematode performance, suggesting that 1OHI3M (or its in planta derivatives *N*-Hex-I3M and *N*-X-I3M) had toxic and/or deterrent effects on nematodes.

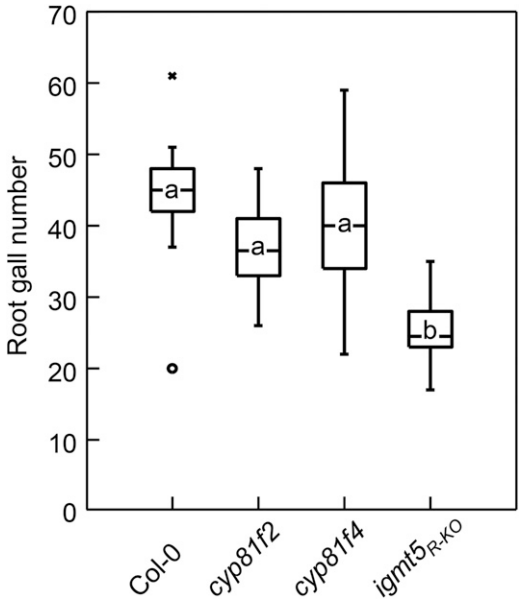

Figure 5. Root gall numbers in the wild type and IG mutants. Shown are means, variances, and outliers in the distribution of root gall numbers on the Col-0 wild type and *cyp81f2*, *cyp81f4*, and $igmt5_{R\text{-}KO}$ genotypes 30 d post inoculation of 1-month-old plants with juvenile nematodes. Ten plants were analyzed per genotype. Different letters indicate significant differences ($P < 0.05$) between genotypes according to posthoc two-tailed Student's t test. The $igmt5_{R\text{-}KO}$ genotype has significantly fewer root galls than the other genotypes (all $t > 4.6$, $P < 0.001$).

DISCUSSION

Biosynthesis of 1MOI3M in Arabidopsis Requires *IGMT5*

In GK_390B09 ($igmt5_{R\text{-}KO}$) roots, the accumulation of 1OHI3M and the near absence of 1MOI3M corresponded with the highly reduced quantity of *IGMT5* transcripts. Vice versa, increased *IGMT5* transcript abundance in SALK_151470 ($IGMT5_{R\text{-}OE}$) roots resulted in an increase in 1MOI3M concentration. Hence, IGMT5 converts 1OHI3M to 1MOI3M. Moreover, disruption of the IGMT5 function in GK_390B09 roots was not compensated for by other IGMTs, even though these enzymes have the potential to convert 1OHI3M to 1MOI3M in a transient *N. benthamiana* expression system (Pfalz et al., 2011). Thus, IGMT5 is the only IGMT that targets 1OHI3M in Arabidopsis. When IGMT5 is nonfunctional, then 1OHI3M and I3M, the metabolic precursors of 1MOI3M, are piling up. Surplus I3M is partly shuttled into the 4-IG modification pathway, resulting in increased 4MOI3M concentration in roots. Surplus 1OHI3M is partially removed by conjugation, resulting in the formation of two conjugates, *N*-Hex-I3M (=c2) and *N*-X-I3M (=c3). Thus, two parallel pathways for IG modification exist, with different but related sets of enzymes being responsible for modification either at position 1 or position 4 of the indole ring. CYP81F4 and IGMT5 carry out hydroxylation and methoxylation at the indole N, whereas CYP81F1 to CYP81F3 and IGMT1 and IGMT2 (and probably also the highly similar IGMT3 and IGMT4) modify the indole ring at position 4 (Fig. 6).

CYP81F4 Expression and IG Transport Processes between Roots and Rosette May Account for Different Leaf Phenotypes of *IGMT5* Promoter Mutants

Both T-DNA insertion mutants had an $IGMT5_{L\text{-}OE}$ genotype; they strongly overexpressed *IGMT5* in their leaves (Figs. 2A and 3A). However, in relation to the strong increase in leaf *IGMT5* transcript levels, alterations in leaf 1MOI3M quantity were fairly moderate (but nonetheless significant; Figs. 2B and 3B). Furthermore, compared with the wild type, 1MOI3M leaf concentration was elevated in SALK_151470 but reduced in GK_390B09. How can these observations be explained?

Previous work had shown that 1MOI3M accumulation strongly depended on *CYP81F4*, the gene coding for the entry enzyme into the 1-IG modification pathway (Pfalz et al., 2011). CYP81F4 activity controls the availability of the IGMT5 substrate 1OHI3M and, in turn, also the abundance of the corresponding reaction product 1MOI3M. Therefore, low expression of *CYP81F4*, as observed in leaves (Figs. 2A and 3A), results in low amounts of 1MOI3M even when *IGMT5* expression is high.

Leaves of GK_390B09 overexpressed *IGMT5* and *CYP81F4* expression was indistinguishable from that of the wild type. Nonetheless, 1MOI3M concentration was

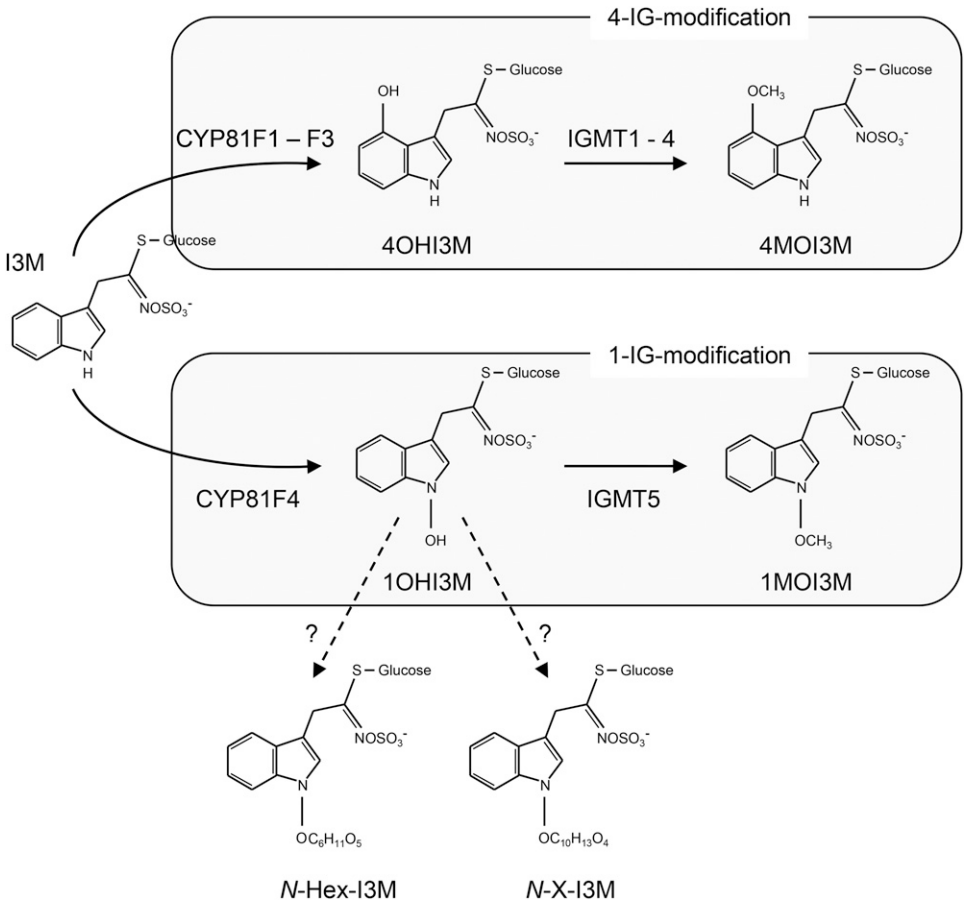

Figure 6. The 4-IG and 1-IG modification pathways in Arabidopsis. Shown are the 4-IG modification pathway (top), the 1-IG modification pathway (middle), and the newly discovered 1OHI3M conjugates (bottom). Inferred enzyme functions are shown next to arrows. The proposed function of IGMT3 and IGMT4 has not yet been demonstrated biochemically. Question marks indicate unknown enzymes. I3M is the product of the IG core pathway. Members of the CYP81F subfamily of cytochrome P450s carry out hydroxylation reactions either in position 4 or 1 of the indole ring. IGMTs belonging to family 2 plant *O*-methyltransferases convert hydroxy intermediates to methoxylated products. IGMT5 is specific for 1OHI3M.

reduced to 50% of the wild-type level (Fig. 3A). Thus, it appears that on-site biosynthesis accounts only partially for leaf 1MOI3M content; the remainder is synthesized in another organ (i.e. the roots) and transported into the leaves. Because GK_390B09 roots are virtually devoid of 1MOI3M (Fig. 3B), they cannot contribute to leaf 1MOI3M accumulation, and the corresponding fraction of 1MOI3M is missing in the leaves. Like GK_390B09, leaves of SALK_151470 overexpressed *IGMT5* and *CYP81F4* transcript levels were unaltered (Fig. 2A), but in contrast to GK_390B09, SALK_151470 overexpressed *IGMT5* also in its roots. Combined with the high, wild-type-like root expression of *CYP81F4* (Fig. 2A), this results in an increase in root and, in turn, via transport to the leaves, also in leaf 1MOI3M concentration (Fig. 2B). Accordingly, the increased 1MOI3M level in SALK_151470 is caused by root (and not leaf) *IGMT5* overexpression.

IG transport between plant organs has been reported previously, and two transporters, GTR1 and GTR2, have been identified as being essential for the transport of Met- and Trp-derived glucosinolates into seeds (Nour-Eldin et al., 2012; Andersen et al., 2013). Noteworthy, these transporters were not required for IG transport between roots and rosette, implying that other, unknown transporters for IG transport exist (Andersen et al., 2013; Jørgensen et al., 2015).

Transport also could explain why *N*-X-I3M is present in the leaves of GK_390B09. As we discuss below, *N*-X-I3M and *N*-Hex-I3M are very likely 1OHI3M detoxification products that are formed when IGMT5 function is disrupted, suggesting that they both originate in $igmt5_{R\text{-}KO}$ roots. However, *N*-Hex-I3M was present only in roots but not in leaves, indicating that IG transport processes may discriminate between different IG structures.

Conjugation of 1OHI3M May Avoid Self-Toxicity Caused by the Disruption of *IGMT5* Function

Plants need to contain potential deleterious, self-toxic effects that may arise from the biosynthesis of defensive metabolites. Among other mechanisms, self-toxicity can be avoided by chemical modification to obtain less reactive metabolites, sequestration of toxic molecules in vacuoles, or excretion into extracellular compartments (for review, see Sirikantaramas et al., 2008). In the case of glucosinolates, self-toxicity is usually avoided by the incorporation of a stabilizing *S*-linked β-D-Glc moiety in the glucosinolate structure and by the compartmentalization of glucosinolates separate from myrosinases, which are specialized thioglucoside glucohydrolases. Myrosinase-catalyzed removal of the

D-Glc moiety generates an unstable intermediate that decomposes rapidly into a variety of bioactive products, such as isothiocyanates, thiocyanates, nitriles, epithionitriles, or oxazolidine-2-thiones (Halkier and Gershenzon, 2006). *S*-Glycosylation and compartmentalization, however, may be insufficient to prevent the potential self-toxicity caused by 1OHI3M. Unsubstituted *N*-hydroxyindoles tend to be highly reactive (Acheson et al., 1974; Acheson, 1990; Somei, 1999). To stabilize these molecules, chemical groups withdrawing electrons from the electron-rich nitrogen of the *N*-hydroxy group or resonance-stabilizing substituents on the indole nucleus are required (Rani and Granchi, 2015). The conversion of the *N*-hydroxy group in 1OHI3M into an *N*-methoxy group, catalyzed by IGMT5, is such a stabilizing reaction. Hence, IGMT5 activity limits 1OHI3M quantity.

Strict control of 1OHI3M abundance in the Arabidopsis wild type is reflected in the tight correlation between *CYP81F4* and *IGMT5* expression across a wide range of tissues, developmental stages, and environmental conditions (Pfalz et al., 2011). But surprisingly, disruption of *IGMT5* expression in GK_390B09 ($igmt5_{R\text{-}KO}$) did not entail a concomitant decrease in *CYP81F4* expression: *CYP81F4* transcript abundance was indistinguishable between GK_390B09 and the wild type (Fig. 3A). Likewise, accumulating 1OHI3M did not provoke a reduction in the accumulation of I3M, 4OHI3M, or 4MOI3M (Fig. 3B). Thus, there is no evidence for negative feedback (Wentzell et al., 2007; Clay et al., 2009) that would reduce flux through the IG core pathway or block entry into the 1-IG modification pathway upon 1OHI3M accumulation. Rather, IG conjugates are formed in GK_390B09 ($igmt5_{R\text{-}KO}$), indicating that this mutant relies on a different mechanism, conjugation, to limit potential hazardous effects that could be caused by accumulating 1OHI3M. Even though attempts to fully elucidate the structure of the I3M conjugates were unsuccessful, evidence from MS analyses supports the conclusion that the substituents are attached to the indole N, thus substituting the reactive *N*-hydroxy group and stabilizing the molecule.

The 1-IG Modification Pathway Can Generate Defense-Related Metabolites

The importance of IGs for aboveground defense against a broad range of enemies is well documented. In vitro and in vivo studies have shown that IGs, in particular those that are modified at position 4 of the indole ring, negatively impacted the performance of the phloem-feeding green peach aphid *Myzus persicae* (Kim and Jander, 2007; Kim et al., 2008; Pfalz et al., 2009). Moreover, IGs influenced the oviposition preferences of crucifer-specialist insects. Intact IGs served as host recognition cues for the diamondback moth *Plutella xylostella* (Sun et al., 2009), and both intact IGs and IG hydrolysis products determined oviposition choices of the butterfly *Pieris rapae* (Huang and Renwick, 1994; de Vos et al., 2008). Likewise, IGs played an important role in defense against fungal, oomycete, and bacterial pathogens, largely attributed to the biosynthesis of CYP81F2-dependent 4-IG modification products and their activation by PEN2 myrosinase-catalyzed hydrolysis (Bednarek et al., 2009; Clay et al., 2009; Hiruma et al., 2010; Sanchez-Vallet et al., 2010; Schlaeppi et al., 2010; Buxdorf et al., 2013; Frerigmann et al., 2016). The CYP81F2/PEN2 pathway is active in leaves but also may contribute to defense against root pathogens (Millet et al., 2010; Iven et al., 2012).

The potential significance of the 1-IG modification pathway for plant-enemy interactions has remained unexplored, even though one of its products, 1MOI3M, is the dominant IG in Arabidopsis roots (Petersen et al., 2002; Brown et al., 2003; Pfalz et al., 2011). We used a soil-borne parasite, the root-knot nematode *M. javanica*, to test whether metabolites from the 1-IG modification pathway contributed to belowground defense. Mutant genotypes suitable for dissecting a potential influence of the 1-IG modification pathway on nematodes, *cyp81f4* and $igmt5_{R\text{-}KO}$, were in the Col-0 background, which had low basal resistance against *M. javanica*. The success of nematode infection and establishment was high in Col-0, indicating that the quantity of 1MOI3M present in roots of this accession posed no major obstacle to *M. javanica*. Consequently, the complete absence of metabolites from the 1-IG modification pathway did not alter nematode success; root gall number on *cyp81f4*, which is defective in the entry enzyme for the 1-IG modification pathway (Fig. 6), was statistically indistinguishable from that of the wild type. By contrast, the number of nematode-induced root galls was reduced significantly in the $igmt5_{R\text{-}KO}$ genotype, indicating that bioactive molecules with nematode-repellent and/or nematode-toxic effects were generated when the 1-IG modification pathway was interrupted at IGMT5. Furthermore, the nematicidal principle required intact *CYP81F4*, because nematode performance on *cyp81f4* did not differ from that on the wild type. Since 4MOI3M accumulated to similar levels in both mutants, $igmt5_{R\text{-}KO}$ and *cyp81f4*, we can rule out that nematicidal effects were caused by this metabolite. Based on the comparison of these two mutants, we also can rule out that the reduction in gall numbers was caused indirectly by altered auxin levels upon disruption of the 1-IG modification pathway (Zhao et al., 2002; Glawischnig et al., 2004). Therefore, we conclude that increased nematode resistance in the $igmt5_{R\text{-}KO}$ genotype was caused by 1OHI3M and/or the partially characterized conjugates *N*-Hex-I3M and *N*-X-I3M, all of which accumulated as a consequence of CYP81F4 activity in the absence of IGMT5 function.

Our results clearly showed that the 1-IG modification pathway had the potential to generate bioactive molecules. Release of this defensive potential required a disruption of the IGMT5 function, which could be triggered by soil-borne parasites in the wild type. Why, then, was this potential not exploited in the Arabidopsis wild type for defense against *M. javanica*? Sedentary

endoparasitic nematodes like *M. javanica* have the ability to suppress their host plant's defenses (Hamamouch et al., 2012; Jaouannet et al., 2013; Xue et al., 2013; for review, see Hewezi and Baum, 2013). Root-knot nematodes require this ability for root entry, migration within the root tissue, and establishment and maintenance of their feeding sites. Feeding site establishment results in the formation of giant cells and, together with a concomitant response of adjacent plant tissue, root gall formation. Indeed, transcript profiles of laser-dissected root galls showed that the IG biosynthesis genes *CYP79B2*, *CYP83B1*, *GGP1*, *SUR1*, *AKN1*, and *IGMT5* and the IG regulator gene *MYB34* were down-regulated in giant cells (Barcala et al., 2010), indicating that IG biosynthesis was suppressed at nematode feeding sites. Vice versa, *CYP79B2*, *IGMT5*, and *MYB34* were up-regulated in intact root galls (Barcala et al., 2010), possibly to limit secondary damage that could arise from nematode-associated pathogens. Hence, root-knot nematode-triggered repression of IG biosynthesis could explain why nematode performance on the Col-0 wild type did not differ from that of *cyp81f4*. However, this would not explain why the $igmt5_{R\text{-}KO}$ genotype was more resistant against nematodes, unless 1OHI3M and/or *N*-Hex-I3M and *N*-X-I3M exerted their effects in the rhizosphere, before or while juvenile nematodes entered the plant roots. Root exudates from cruciferous plants indeed contain glucosinolates and glucosinolate hydrolysis products (Schreiner et al., 2011; Strehmel et al., 2014), and these metabolites have the potential to alter soil microbial communities (Bressan et al., 2009).

Even though 1MOI3M did not alter the performance of *M. javanica*, this does not preclude a function of this metabolite in defense against other soil-borne parasites in Arabidopsis or other crucifers. Indeed, *IGMT5* has been suggested as a candidate gene for a *Sclerotinia* spp. stem rot resistance quantitative trait locus in *Brassica napus* (Wu et al., 2013). In terms of chemical reactivity, the methoxy group at the indole N serves to stabilize the corresponding isothiocyanate and the downstream alcohol originating from spontaneous hydrolysis (Hanley et al., 1990). By this effect, the *N*-methoxy group could influence the quantitative balance of the complex mixture of hydrolysis products that originate from myrosinase-catalyzed hydrolysis as well as the actual resulting structures and bioactivities (Agerbirk et al., 1996, 1998; Stephensen et al., 2000).

Further biodiversity has been discovered as 1- and 4-substituted indole phytoalexins in various crucifers (Pedras et al., 2010, 2011) and as the rare disubstituted 1,4-dimethoxy I3M in *Barbarea vulgaris* (Agerbirk et al., 2001). From the growing amount of bioinformatics data in chemical ecology model systems (Liu et al., 2016) and the biochemical data from Arabidopsis, structural variants such as these can be tested for complementary resistance properties. Similarly, translational research with *Brassica* spp. vegetables will allow precise testing of the nutritional effects of IG nitrogen substitution (Schumacher et al., 2014; Wiesner et al., 2014). With the characterization of mutants for *CYP81F4* (Pfalz et al., 2011) and *IGMT5* (this work), the tools necessary to determine the significance of the 1-IG modification pathway for plant-enemy and vegetable-human interactions are now at hand.

MATERIALS AND METHODS

Plant Growth Conditions

Arabidopsis (*Arabidopsis thaliana*) lines SALK_151470 (accession no. N437365; Alonso et al., 2003) and GK_390B09 (accession no. N651470; Kleinboelting et al., 2012) were obtained from the Nottingham Arabidopsis Stock Centre. For the analysis of glucosinolates and for RNA extraction prior to RT-qPCR, Arabidopsis seeds were sown into damp potting medium, cold treated at 6°C in the dark for 3 to 4 d, and germinated in the light. Plants were grown in an environmentally controlled growth chamber equipped with T8 LUXLINE PLUS F58W/865 bulbs (Sylvania) with 200 μmol s^{-1} m^{-2} as a light source, with an 11.5-h-day/12.5-h-night cycle, and 22°C and 60% relative humidity (day) and 16°C and 75% relative humidity (night). Seedlings were transferred to sand (particle size of 2 mm or less; Sacamat sable fin 0/2) 5 to 7 d post germination. Every 7 to 10 d, plants were fertilized with 30 mL of 0.1% (v/v) Hydrocani C2 liquid fertilizer (Hydro Agri). For nematode bioassays, Arabidopsis seeds were surface sterilized and sown onto petri dishes with one-half-strength Murashige and Skoog medium + B5 vitamin Gamborg, 1% (w/v) plant agar, 1% (w/v) Suc (all Duchefa Biochimie), and 0.1% (w/v) MES (Carl Roth), adjusted to pH 5.7. Following cold treatment and germination in the light, seedlings were transferred to sand 10 to 12 d post germination.

DNA Extraction and Genotyping

Isolation of DNA from freeze-dried Arabidopsis leaves was described previously (Kroymann et al., 2001). Seed material for GK_390B09 and SALK_151470 provided by the Nottingham Arabidopsis Stock Centre was segregating for the T-DNA insertion. T3 plants were screened with PCR-based markers to identify lines with either homozygous mutant or homozygous wild-type alleles. Primers are listed in Supplemental Table S1. For GK_390B09, primer combination GABI_390F + GABI_390R was specific for the wild type and primer combination GABI_390R + GABI-Lb1 was specific for mutant alleles. For SALK_151470, primer combination 151470F + 151470R was specific for the wild type and primer combination 151470R + LB1 was specific for mutant alleles. PCR-based genotyping was carried out as described by Pfalz et al. (2011).

RNA Extraction and RT-qPCR

Leaves and roots were ground to a fine powder. Tissue samples were cooled with liquid N_2 during processing to prevent RNA degradation. Total RNA was extracted with TRIsure reagent (Bioline) following the manufacturer's recommendations, treated with DNase (Turbo DNase; Ambion), and purified with RNeasy MinElute columns (Qiagen). RNA integrity was verified with RNA Nano chips (Agilent Technologies) on an Agilent 2100 Bioanalyzer. RNA quantity was determined with a Nanodrop ND-1000 spectrophotometer (Nanodrop Technologies). First-strand cDNA synthesis from a maximum of 500 ng of DNA-free total RNA was carried out with the Maxima First Strand cDNA Synthesis Kit (ThermoFisher) according to the manufacturer's recommendations. RT-qPCR was performed with Maxima SYBR Green qPCR Master Mix (ThermoFisher) on the StepOnePlus Real Time PCR System (Applied Biosystems) with an initial denaturation for 10 min at 94°C, followed by 40 cycles of 15 s at 94°C, 30 s at 58°C, and 30 s at 72°C. RT-qPCR data were analyzed with qbase$^+$ (Biogazelle).

Glucosinolate Extraction and HPLC Analysis in a 96-Well Format

Wild-type (Col-0) and mutant plants were randomized and grown in sand. Roots and leaves from 4-week-old plants were harvested separately. Roots were rinsed briefly with water to remove attached sand and dried quickly with a paper towel. The fresh weight of leaves and roots was determined, and samples were snap frozen in liquid N_2. Tissue was lyophilized to dryness and homogenized

with 2.3-mm ball bearings in a shaker. Extraction of glucosinolates in their desulfated form was carried out as described by Pfalz et al. (2011) but without adding an internal standard. Desulfoglucosinolates were separated on the Dionex UltiMate 3000 Rapid Separation LC System equipped with a LiChrospher 100 RP-18 end-capped LiChroCART column (4 × 250 mm; pore size, 100 A; particle size, 5 μm). HPLC separation, desulfoglucosinolate identification based on retention times, and diode array UV light detection were conducted as described by Kroymann et al. (2001). Integrated peak area at UV_{229nm} was corrected for dilution and sample weight. Data for wild-type and mutant root and leaf glucosinolate profiles were analyzed with Systat version 9 (SPSS) using a general linear model: glucosinolate = constant + genotype + row + column, with row and column as variables to control for position effects during plant growth and desulfoglucosinolate extraction in a 96-well format.

HPLC-MS/MS of Desulfated Glucosinolates

The identification of newly discovered IG derivatives in Arabidopsis *igmt5* roots was attempted using an established, gentle method based on extraction in boiling aqueous methanol, binding to anion-exchange columns, enzymatic desulfation, and preparative HPLC with a Luna C18 (2) column (250 mm × 4.6 mm, 5 μm; Phenomenex) with diode array UV light detection followed by either ion-trap HPLC-MS/MS using NaCl-doped eluent or lyophilization plus ^{1}H-NMR at 400 MHz in deuterium oxide (Agerbirk and Olsen, 2011). The sulfatase enzyme was partially purified by fractional precipitation (Graser et al., 2001) from a commercially obtained *Helix pomatia* enzyme powder known to contain other hydrolytic activities, including glucuronidase (S9626; Sigma-Aldrich). Known glucosinolates in the samples were identified in parallel based on comparisons of UV light spectra, retention times, m/z values, and MS^2 results with those of authentic desulfated standards including known IG (Agerbirk et al., 2001) and, in one case, by NMR as a positive control (desulfo 4-methylsulfinylbutyl glucosinolate). Additional HR-MS of desulfoglucosinolates was carried out using a Bruker Compact electrospray ionization-quadrupole-time of flight instrument (Bruker Daltonics). The attempted isolation of IG derivatives as intact glucosinolates was carried out as reported previously (Agerbirk et al., 2014), except that the acidic wash was left out in an attempt to avoid degradation.

HR-MS of Intact Glucosinolates

Samples were homogenized for 5 min in 2.5 mL of 3:1 (v/v) acetonitrile:water using a Polytron homogenizer (Fisher Scientific) and centrifuged for 15 min and 20°C at 8,000*g*. Supernatants were collected. The pellets were reextracted with 1 mL of 3:1 (v/v) acetonitrile:water and sonicated (15 min, 25 Hz). After centrifugation, supernatants from the first and second extractions were pooled. Extracts were evaporated to dryness at ambient temperature in a Thermo Savant SpeedVac. Dried extracts were dissolved in 1:19 (v/v) acetonitrile:water and filtered. Liquid chromatography-HR-MS analysis was carried out on an I-class ultra-performance liquid chromatography system coupled with a Xevo G2-S QToF mass spectrometer (Waters). Liquid chromatography separation was conducted at 40°C on a Waters ACQUITY UPLC CSH C18 column (2.1 × 100 mm length, 1.7 μm) using an acetonitrile (+0.1% formic acid)/water (+0.1% formic acid) gradient as a mobile phase. MS data were acquired in negative electrospray, resolution mode (32,000 FWHM) and by MS and MS^E modes. Leucine enkephalin was used as lockspray. The electrospray capillary potential was 1.5 kV. The source block and desolvation gas had temperatures of 110°C and 450°C, respectively. N_2 was used as nebulization gas and desolvation gas (100 and 800 L h^{-1}, respectively). Collision-induced dissociation MS^E experiments were performed using a 20- to 55-eV collision energy ramp.

Nematode Assays

A *Meloidogyne javanica* population was maintained on tomato (*Solanum lycopersicum*) plants of the nematode-susceptible variety Roma, grown in 20-cm-square pots filled with 2:1 (v/v) sand (particle size, 2 mm; Sacamat): potting soil in climate chambers (Pol-EkoAparatura-type kk 1200 STD; Wodzisław Śląski-Pologne) with a 14-h-day/10-h-night cycle at 28°C and 65% relative humidity (day) and 19°C and 65% relative humidity (night). Nematode eggs were collected and placed on a small mesh (mesh size > 200 μm) floating on distilled water in a petri dish. Eggs were placed for 1 week in the dark at 28°C, after which nematode juvenile larvae had hatched. Nematode number was estimated with nematode-counting slides (Chalex) and a stereomicroscope, and the nematode concentration was adjusted to approximately 50 to 100 mL^{-1}. Arabidopsis plants were inoculated with 1 mL of nematode suspension per plant 1 month after plants had been transferred to sand. Thirty days after inoculation with nematodes, plant roots were carefully washed with water and dispersed in a flat dish, and the total number of galls formed on the roots was counted with the help of a stereomicroscope.

Accession Numbers

Sequence data from this article can be found in the Arabidopsis Genome Initiative database under accession numbers At1g76790 (*IGMT5*), At4g37410 (*CYP81F4*), At1g21100 (*IGMT1*), At1g21120 (*IGMT2*), At1g21110 (*IGMT3*), and At1g21130 (*IGMT4*).

Supplemental Data

The following supplemental materials are available.

Supplemental Figure S1. HPLC profiles and UV light absorption spectra of desulfated glucosinolates extracted from roots of Col-0 and GK_390B09 ($igmt5_{R\text{-}KO}$).

Supplemental Figure S2. Quantity and stability of desulfated IGs during HPLC analysis.

Supplemental Figure S3. Desulfated glucosinolates from Arabidopsis $igmt5_{R\text{-}KO}$ roots analyzed by HPLC-MS/MS.

Supplemental Table S1. Primers used in this study.

ACKNOWLEDGMENTS

We thank Dr. Thierry Mateille from the Centre de Biologie pour la Gestion des Populations for supplying *M. javanica*.

Received September 7, 2016; accepted October 31, 2016; published November 3, 2016.

LITERATURE CITED

Acheson RM (1990) 1-Hydroxypyrroles, 1-hydroxyindoles and 9-hydroxycarbazoles. Adv Heterocycl Chem **51:** 105–175

Acheson RM, Littlewood DM, Rosenberg HE (1974) Synthesis of 1-methoxyindoles. J Chem Soc Chem Commun **16:** 671

Agerbirk N, Bjergegaard C, Olsen CE, Sørensen H (1996) Kinetic investigation of the transformations of indol-3-ylcarbinol into oligomeric indolyl compounds based on micellar electrokinetic capillary chromatography. J Chromatogr A **745:** 239–248

Agerbirk N, De Vos M, Kim JH, Jander G (2009) Indole glucosinolate breakdown and its biological effects. Phytochem Rev **8:** 101–120

Agerbirk N, Olsen CE (2011) Isoferuloyl derivatives of five seed glucosinolates in the crucifer genus Barbarea. Phytochemistry **72:** 610–623

Agerbirk N, Olsen CE (2012) Glucosinolate structures in evolution. Phytochemistry **77:** 16–45

Agerbirk N, Olsen CE, Cipollini D, Ørgaard M, Linde-Laursen I, Chew FS (2014) Specific glucosinolate analysis reveals variable levels of epimeric glucobarbarins, dietary precursors of 5-phenyloxazolidine-2-thiones, in watercress types with contrasting chromosome numbers. J Agric Food Chem **62:** 9586–9596

Agerbirk N, Olsen CE, Sørensen H (1998) Initial and final products, nitriles, and ascorbigens produced in myrosinase-catalyzed hydrolysis of indole glucosinolates. J Agric Food Chem **46:** 1563–1571

Agerbirk N, Petersen BL, Olsen CE, Halkier BA, Nielsen JK (2001) 1,4-Dimethoxyglucobrassicin in Barbarea and 4-hydroxyglucobrassicin in Arabidopsis and Brassica. J Agric Food Chem **49:** 1502–1507

Alonso JM, Stepanova AN, Leisse TJ, Kim CJ, Chen H, Shinn P, Stevenson DK, Zimmerman J, Barajas P, Cheuk R, et al (2003) Genome-wide insertional mutagenesis of *Arabidopsis thaliana*. Science **301:** 653–657

Andersen TG, Nour-Eldin HH, Fuller VL, Olsen CE, Burow M, Halkier BA (2013) Integration of biosynthesis and long-distance transport establish organ-specific glucosinolate profiles in vegetative *Arabidopsis*. Plant Cell **25:** 3133–3145

Barcala M, García A, Cabrera J, Casson S, Lindsey K, Favery B, García-Casado G, Solano R, Fenoll C, Escobar C (2010) Early transcriptomic events in microdissected Arabidopsis nematode-induced giant cells. Plant J **61:** 698–712

Bednarek P, Piślewska-Bednarek M, Svatoš A, Schneider B, Doubský J, Mansurova M, Humphry M, Consonni C, Panstruga R, Sanchez-Vallet A, et al (2009) A glucosinolate metabolism pathway in living plant cells mediates broad-spectrum antifungal defense. Science **323:** 101–106

Bialecki JB, Ruzicka J, Weisbecker CS, Haribal M, Attygalle AB (2010) Collision-induced dissociation mass spectra of glucosinolate anions. J Mass Spectrom **45:** 272–283

Bressan M, Roncato MA, Bellvert F, Comte G, Haichar FZ, Achouak W, Berge O (2009) Exogenous glucosinolate produced by *Arabidopsis thaliana* has an impact on microbes in the rhizosphere and plant roots. ISME J **3:** 1243–1257

Brown PD, Tokuhisa JG, Reichelt M, Gershenzon J (2003) Variation of glucosinolate accumulation among different organs and developmental stages of *Arabidopsis thaliana*. Phytochemistry **62:** 471–481

Buxdorf K, Yaffe H, Barda O, Levy M (2013) The effects of glucosinolates and their breakdown products on necrotrophic fungi. PLoS ONE **8:** e70771

Clay NK, Adio AM, Denoux C, Jander G, Ausubel FM (2009) Glucosinolate metabolites required for an Arabidopsis innate immune response. Science **323:** 95–101

de Vos M, Kriksunov KL, Jander G (2008) Indole-3-acetonitrile production from indole glucosinolates deters oviposition by *Pieris rapae*. Plant Physiol **146:** 916–926

Fabre N, Poinsot V, Debrauwer L, Vigor C, Tulliez J, Fourasté I, Moulis C (2007) Characterisation of glucosinolates using electrospray ion trap and electrospray quadrupole time-of-flight mass spectrometry. Phytochem Anal **18:** 306–319

Frerigmann H, Piślewska-Bednarek M, Sánchez-Vallet A, Molina A, Glawischnig E, Gigolashvili T, Bednarek P (2016) Regulation of pathogen-triggered tryptophan metabolism in *Arabidopsis thaliana* by MYB transcription factors and indole glucosinolate conversion products. Mol Plant **9:** 682–695

Giamoustaris A, Mithen R (1996) Genetics of aliphatic glucosinolates. IV. Side-chain modification in *Brassica oleracea*. Theor Appl Genet **93:** 1006–1010

Glawischnig E, Hansen BG, Olsen CE, Halkier BA (2004) Camalexin is synthesized from indole-3-acetaldoxime, a key branching point between primary and secondary metabolism in Arabidopsis. Proc Natl Acad Sci USA **101:** 8245–8250

Graser G, Oldham NJ, Brown PD, Temp U, Gershenzon J (2001) The biosynthesis of benzoic acid glucosinolate esters in *Arabidopsis thaliana*. Phytochemistry **57:** 23–32

Halkier BA, Gershenzon J (2006) Biology and biochemistry of glucosinolates. Annu Rev Plant Biol **57:** 303–333

Hamamouch N, Li C, Hewezi T, Baum TJ, Mitchum MG, Hussey RS, Vodkin LO, Davis EL (2012) The interaction of the novel 30C02 cyst nematode effector protein with a plant β-1,3-endoglucanase may suppress host defence to promote parasitism. J Exp Bot **63:** 3683–3695

Hanley AB, Parsley KR, Lewis JA, Fenwick GR (1990) Chemistry of indole glucosinolates: intermediacy of indol-3-ylmethyl isothiocyanates in the enzymatic hydrolysis of indole glucosinolates. J Chem Soc Perkin Trans **8:** 2273–2276

Hewezi T, Baum TJ (2013) Manipulation of plant cells by cyst and root-knot nematode effectors. Mol Plant Microbe Interact **26:** 9–16

Hiruma K, Onozawa-Komori M, Takahashi F, Asakura M, Bednarek P, Okuno T, Schulze-Lefert P, Takano Y (2010) Entry mode-dependent function of an indole glucosinolate pathway in *Arabidopsis* for nonhost resistance against anthracnose pathogens. Plant Cell **22:** 2429–2443

Huang X, Renwick JAA (1994) Relative activities of glucosinolates as oviposition stimulants for *Pieris rapae* and *P. napi oleracea*. J Chem Ecol **20:** 1025–1037

Iven T, König S, Singh S, Braus-Stromeyer SA, Bischoff M, Tietze LF, Braus GH, Lipka V, Feussner I, Dröge-Laser W (2012) Transcriptional activation and production of tryptophan-derived secondary metabolites in Arabidopsis roots contributes to the defense against the fungal vascular pathogen *Verticillium longisporum*. Mol Plant **5:** 1389–1402

Jaouannet M, Magliano M, Arguel MJ, Gourgues M, Evangelisti E, Abad P, Rosso MN (2013) The root-knot nematode calreticulin Mi-CRT is a key effector in plant defense suppression. Mol Plant Microbe Interact **26:** 97–105

Jørgensen ME, Nour-Eldin HH, Halkier BA (2015) Transport of defense compounds from source to sink: lessons learned from glucosinolates. Trends Plant Sci **20:** 508–514

Kim BG, Kim DH, Hur HG, Lim J, Lim Y, Ahn JH (2005) O-Methyltransferases from *Arabidopsis thaliana*. Agric Chem Biotechnol **48:** 113–119

Kim JH, Jander G (2007) *Myzus persicae* (green peach aphid) feeding on Arabidopsis induces the formation of a deterrent indole glucosinolate. Plant J **49:** 1008–1019

Kim JH, Lee BW, Schroeder FC, Jander G (2008) Identification of indole glucosinolate breakdown products with antifeedant effects on *Myzus persicae* (green peach aphid). Plant J **54:** 1015–1026

Kleinboelting N, Huep G, Kloetgen A, Viehoever P, Weisshaar B (2012) GABI-Kat SimpleSearch: new features of the *Arabidopsis thaliana* T-DNA mutant database. Nucleic Acids Res **40:** D1211–D1215

Kliebenstein DJ, Kroymann J, Brown P, Figuth A, Pedersen D, Gershenzon J, Mitchell-Olds T (2001a) Genetic control of natural variation in Arabidopsis glucosinolate accumulation. Plant Physiol **126:** 811–825

Kliebenstein DJ, Lambrix VM, Reichelt M, Gershenzon J, Mitchell-Olds T (2001b) Gene duplication in the diversification of secondary metabolism: tandem 2-oxoglutarate-dependent dioxygenases control glucosinolate biosynthesis in *Arabidopsis*. Plant Cell **13:** 681–693

Kroymann J, Donnerhacke S, Schnabelrauch D, Mitchell-Olds T (2003) Evolutionary dynamics of an Arabidopsis insect resistance quantitative trait locus. Proc Natl Acad Sci USA (Suppl 2) **100:** 14587–14592

Kroymann J, Textor S, Tokuhisa JG, Falk KL, Bartram S, Gershenzon J, Mitchell-Olds T (2001) A gene controlling variation in Arabidopsis glucosinolate composition is part of the methionine chain elongation pathway. Plant Physiol **127:** 1077–1088

Latté KP, Appel KE, Lampen A (2011) Health benefits and possible risks of broccoli: an overview. Food Chem Toxicol **49:** 3287–3309

Liu T, Zhang X, Yang H, Agerbirk N, Qiu Y, Wang H, Shen D, Song J, Li X (2016) Aromatic glucosinolate biosynthesis pathway in *Barbarea vulgaris* and its response to *Plutella xylostella* infestation. Front Plant Sci **7:** 83

Magrath R, Bano F, Morgner M, Parkin I, Sharpe A, Lister C, Dean C, Turner J, Lydiate D, Mithen R (1994) Genetics of aliphatic glucosinolates. I. Side chain elongation in *Brassica napus* and *Arabidopsis thaliana*. Heredity **72:** 290–299

Millet YA, Danna CH, Clay NK, Songnuan W, Simon MD, Werck-Reichhart D, Ausubel FM (2010) Innate immune responses activated in *Arabidopsis* roots by microbe-associated molecular patterns. Plant Cell **22:** 973–990

Nour-Eldin HH, Andersen TG, Burow M, Madsen SR, Jørgensen ME, Olsen CE, Dreyer I, Hedrich R, Geiger D, Halkier BA (2012) NRT/PTR transporters are essential for translocation of glucosinolate defence compounds to seeds. Nature **488:** 531–534

Pedras MSC, Yaya EE, Glawischnig E (2011) The phytoalexins from cultivated and wild crucifers: chemistry and biology. Nat Prod Rep **28:** 1381–1405

Pedras MSC, Yaya EE, Hossain S (2010) Unveiling the phytoalexin biosynthetic puzzle in salt cress: unprecedented incorporation of glucobrassicin into wasalexins A and B. Org Biomol Chem **8:** 5150–5158

Petersen BL, Chen S, Hansen CH, Olsen CE, Halkier BA (2002) Composition and content of glucosinolates in developing *Arabidopsis thaliana*. Planta **214:** 562–571

Pfalz M, Mikkelsen MD, Bednarek P, Olsen CE, Halkier BA, Kroymann J (2011) Metabolic engineering in *Nicotiana benthamiana* reveals key enzyme functions in *Arabidopsis* indole glucosinolate modification. Plant Cell **23:** 716–729

Pfalz M, Vogel H, Kroymann J (2009) The gene controlling the Indole Glucosinolate Modifier1 quantitative trait locus alters indole glucosinolate structures and aphid resistance in *Arabidopsis*. Plant Cell **21:** 985–999

Rani R, Granchi C (2015) Bioactive heterocycles containing endocyclic N-hydroxy groups. Eur J Med Chem **97:** 505–524

Sanchez-Vallet A, Ramos B, Bednarek P, López G, Piślewska-Bednarek M, Schulze-Lefert P, Molina A (2010) Tryptophan-derived secondary metabolites in *Arabidopsis thaliana* confer non-host resistance to necrotrophic *Plectosphaerella cucumerina* fungi. Plant J **63:** 115–127

Schlaeppi K, Abou-Mansour E, Buchala A, Mauch F (2010) Disease resistance of Arabidopsis to *Phytophthora brassicae* is established by the sequential action of indole glucosinolates and camalexin. Plant J **62:** 840–851

Schreiner M, Krumbein A, Knorr D, Smetanska I (2011) Enhanced glucosinolates in root exudates of *Brassica rapa* ssp. rapa mediated by salicylic acid and methyl jasmonate. J Agric Food Chem **59:** 1400–1405

Schumacher F, Florian S, Schnapper A, Monien BH, Mewis I, Schreiner M, Seidel A, Engst W, Glatt H (2014) A secondary metabolite of Brassicales, 1-methoxy-3-indolylmethyl glucosinolate, as well as its degradation product, 1-methoxy-3-indolylmethyl alcohol, forms DNA adducts in the mouse, but in varying tissues and cells. Arch Toxicol **88:** 823–836

Sirikantaramas S, Yamazaki M, Saito K (2008) Mechanisms of resistance to self-produced toxic secondary metabolites in plants. Phytochem Rev **7:** 467–477

Somei M (1999) 1-Hydroxyindoles. Heterocycles **50:** 1157–1211

Sønderby IE, Geu-Flores F, Halkier BA (2010) Biosynthesis of glucosinolates: gene discovery and beyond. Trends Plant Sci **15:** 283–290

Stephensen PU, Bonnesen C, Schaldach C, Andersen O, Bjeldanes LF, Vang O (2000) N-Methoxyindole-3-carbinol is a more efficient inducer of cytochrome P-450 1A1 in cultured cells than indol-3-carbinol. Nutr Cancer **36:** 112–121

Strehmel N, Böttcher C, Schmidt S, Scheel D (2014) Profiling of secondary metabolites in root exudates of *Arabidopsis thaliana*. Phytochemistry **108:** 35–46

Sun JY, Sønderby IE, Halkier BA, Jander G, de Vos M (2009) Non-volatile intact indole glucosinolates are host recognition cues for ovipositing *Plutella xylostella*. J Chem Ecol **35:** 1427–1436

Wentzell AM, Rowe HC, Hansen BG, Ticconi C, Halkier BA, Kliebenstein DJ (2007) Linking metabolic QTLs with network and cis-eQTLs controlling biosynthetic pathways. PLoS Genet **3:** 1687–1701

Wiesner M, Schreiner M, Zrenner R (2014) Functional identification of genes responsible for the biosynthesis of 1-methoxy-indol-3-ylmethyl-glucosinolate in *Brassica rapa* ssp. chinensis. BMC Plant Biol **14:** 124

Wu J, Cai G, Tu J, Li L, Liu S, Luo X, Zhou L, Fan C, Zhou Y (2013) Identification of QTLs for resistance to sclerotinia stem rot and BnaC. IGMT5.a as a candidate gene of the major resistant QTL SRC6 in *Brassica napus*. PLoS ONE **8:** e67740

Wu Y, Jenkins T, Blunden G, von Mende N, Hankins SD (1998) Suppression of fecundity of the root-knot nematode, Meloidogyne javanica, in monoxenic cultures of *Arabidopsis thaliana* treated with an alkaline extract of *Ascophyllum nodosum*. J Appl Phycol **10:** 91–94

Xue B, Hamamouch N, Li C, Huang G, Hussey RS, Baum TJ, Davis EL (2013) The 8D05 parasitism gene of *Meloidogyne incognita* is required for successful infection of host roots. Phytopathology **103:** 175–181

Zhao Y, Hull AK, Gupta NR, Goss KA, Alonso J, Ecker JR, Normanly J, Chory J, Celenza JL (2002) Trp-dependent auxin biosynthesis in Arabidopsis: involvement of cytochrome P450s CYP79B2 and CYP79B3. Genes Dev **16:** 3100–3112